Distributed Reflectivity Solar Sails for Extended Mission Applications

Andreas Borggräfe[1] and Jeannette Heiligers[2]
Advanced Space Concepts Laboratory, Department of Mechanical and Aerospace Engineering, University of Strathclyde, Glasgow, G4 0LT, United Kingdom

Matteo Ceriotti[3]
School of Engineering, James Watt South Building, University of Glasgow, Glasgow, G12 8QQ, United Kingdom

and

Colin R. McInnes[4]
Advanced Space Concepts Laboratory, Department of Mechanical and Aerospace Engineering, University of Strathclyde, Glasgow, G4 0LT, United Kingdom

The dynamics of solar sails with a variable surface reflectivity distribution are investigated. When changing the reflectivity across the sail film, solar radiation pressure forces and torques can be controlled without changing the attitude of the spacecraft relative to the Sun or using attitude control actuators. The reflectivity can in principle be modified using electro-chromic coatings, which are applied here as examples to counteract gravity-gradient torques in Earth orbit and to enable specific shape profiles of a flexible sail film. This 'optical reconfiguration' method introduces an adaptive solar sail as a multi-functional platform for novel mission applications.

I. Introduction

USING conventional solar sailing technology, the solar radiation pressure (SRP) force vector direction and magnitude depend strongly on the sail attitude relative to the Sun, limiting the applicability of solar sails compared to other low-thrust propulsion systems such as solar-electric propulsion. Furthermore, the SRP force magnitude follows an inverse square law with solar distance, making the sail less efficient at large distances from the Sun [1]. In order to increase the flexibility of modulating the SRP forces and torques and to increase the range of potential solar sail mission applications, we introduce the concepts of shape change and variable optical

[1] PhD Researcher, Department of Mechanical and Aerospace Engineering, 141 St James Road, Lord Hope Building, University of Strathclyde, Glasgow, G4 0LT
[2] Research Associate, Department of Mechanical and Aerospace Engineering, 141 St James Road, Lord Hope Building, University of Strathclyde, Glasgow, G4 0LT
[3] Lecturer, School of Engineering, James Watt South Building, University of Glasgow, G12 8QQ, Glasgow
[4] Professor, Department of Mechanical and Aerospace Engineering, 141 St James Road, Lord Hope Building, University of Strathclyde, Glasgow, G4 0LT

properties for large gossamer spacecraft [2]. Merging these concepts, potential benefits of such a system over conventional solar sails can be identified. It is envisaged to use future shape-changing solar sails as multi-functional platforms that can deliver additional key mission functionality such as power collection, sensing and communications. For example, the sail may begin at Earth escape in a flat configuration on a small-body science mission towards a designated target object. In close proximity to the target body, the sail reconfigures to a parabolic shape, using its reflective film as a remote sensing device or as a large communication antenna, before continuing again in a flat thrust mode.

To demonstrate these capabilities of solar sails, this paper investigates the use of variable film reflectivity for attitude and deflection control. First, in Section II, the attitude dynamics of a rigid, flat solar sail with a variable surface reflectivity distribution will be investigated. When changing the reflectivity coefficient across the sail film, the SRP forces and torques acting on the sail can be controlled without changing the incidence angle relative to the Sun and without using additional attitude control actuators. The reflectivity can be modified using electro-chromic coatings, which consist of an electro-active material that changes its surface reflectivity according to an applied electric potential [3]. By assigning an appropriate reflectivity function across the sail area, the center-of-pressure can be shifted optically relative to the center-of-mass (CoM), rather than mechanically, as for example through the use of moving payload masses. This enables more flexible steering of the solar sail and minimizes actuation effort.

Subsequently, in Section III, a variable reflectivity distribution is used to control the deflection of a flexible sail film due to the transverse SRP load acting on the surface. The very thin membrane-like sail film experiences relatively high deflections from the initially flat shape and requires the use of non-linear flexible bending theory [4], accounting for the non-negligible in-plane tension within the material. The deflection magnitudes and shapes due to a constant surface reflectivity are presented for various circular sail films of different radius and distances from the Sun. The nominal deflection shapes are then manipulated through the use of suitable reflectivity functions across the surface. It is shown that when a particular deflection shape is selected a priori (e.g. a parabolic one to achieve the remote sensing device and/or antenna as mentioned above), the required reflectivity distribution can be calculated by formulating an inverse problem. Resulting paraboloid-type deflection shapes and deflection magnitudes are assessed in Section IV in terms of their usefulness for novel mission applications for solar sails, using shape-changing reflective sail films.

II. Sail Attitude Control using Variable Reflectivity Distribution

As a first example, a variable reflectivity distribution is used to control the attitude of a solar sail in low Earth orbit (LEO). In particular, this steering method is applied to counteract the gravity-gradient torques acting on a large rigid sail film. It will be shown that a constant Sun-pointing attitude can be maintained along the orbit, while likewise minimizing the necessary surface reflectivity. A square solar sail is modeled as a rigid flat Kapton® film of density $\delta = 1{,}572\ \mathrm{kg/m^3}$ [5], thickness $d = 2.5\times10^{-6}\,\mathrm{m}$ and edge length $L = 50\ \mathrm{m}$, without assembly or payload masses, as shown in Fig. 1.

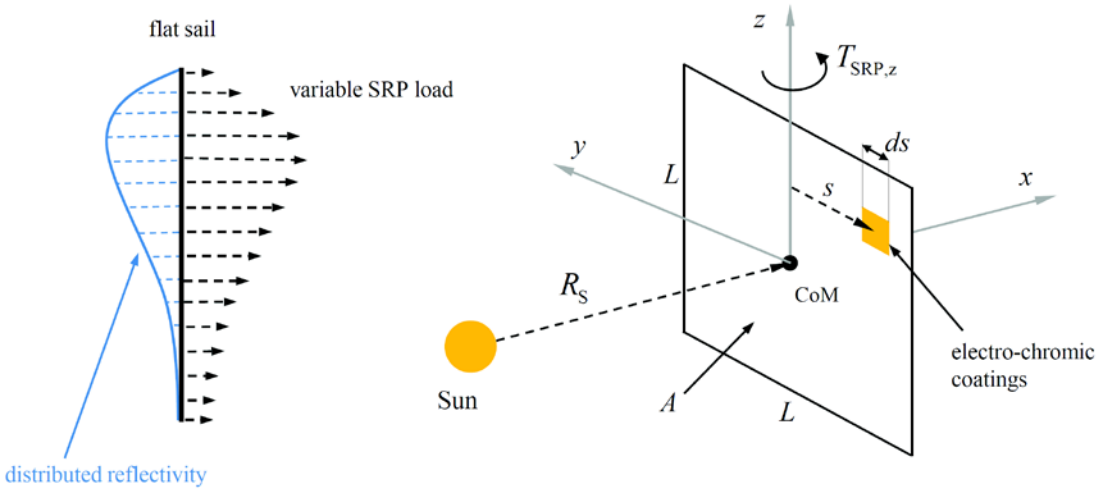

Fig. 1 Square flat solar sail with variable reflectivity distribution across the surface (left) and sail model using patched electro-chromic elements (right)

A sail-fixed Cartesian coordinate frame (**x**,**y**,**z**) is used to describe the sail attitude along its orbit, where the **z**-axis is constrained to be always perpendicular to the ecliptic plane. This allows only one degree of rotational freedom, while rotation about the sail **x** and **y** axes is omitted. The mass moments of inertia of the Kapton® film are $I_{xx} = 4093.8\ \mathrm{kg\,m^2}$ and $I_{yy} = I_{zz} = 2046.9\ \mathrm{kg\,m^2}$, with a total mass $m = 9.83\ \mathrm{kg}$. It is ideally assumed that the entire sail area A is covered with electro-chromic coating elements that are able to change their reflectivity. The additional mass and thickness of the elements is neglected throughout this preliminary study. When changing the reflectivity of a surface element $dA = L \cdot ds$ on the sail, where s denotes the distance of the element from the axis of rotation, the difference in SRP force creates a torque about the CoM of the sail.

The CoM of the sail is assumed to move on a circular LEO of 400 km altitude in the ecliptic plane, as shown in Fig. 2, while air drag and solar eclipses are ignored for illustration. A constant sail cone angle $\alpha = 0$ deg between the Sun-sail line $\mathbf{R}_S$ and the sail plane normal is assumed.

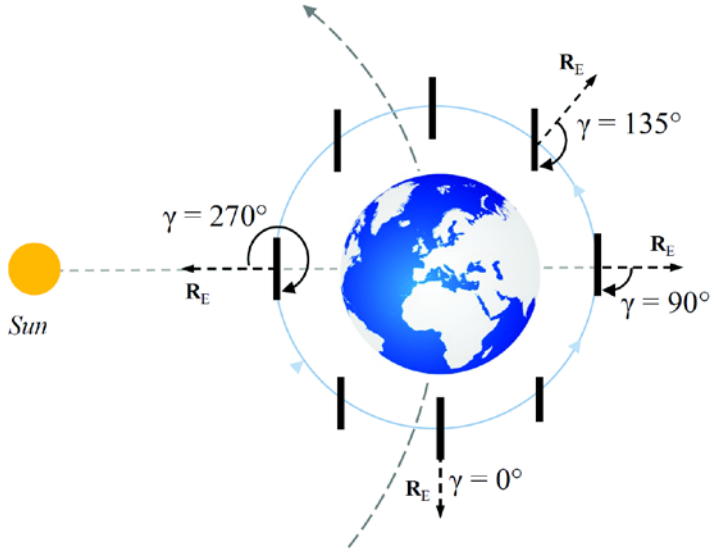

Fig. 2 Rigid flat solar sail on Earth-centered circular LEO of 400 km altitude and constant Sun-pointing attitude

The gravity-gradient torque along the orbit depends on the angle γ between the sail plane and the Earth radial direction $\mathbf{R}_{\mathrm{E}}$. It can be approximated using the standard relation

$$T_{\mathrm{GG,z}} = 3\frac{\mu_E}{R_{\mathrm{CoM}}^3}\sin\gamma\cos\gamma\ (I_{\mathrm{xx}} - I_{\mathrm{yy}}) \tag{1}$$

with μ_E being the gravitational parameter of the Earth and R_{CoM} the radial distance of the sail's CoM from the Earth's center [6]. For example, the maximum gravity-gradient torque acting on the sail considered here is of the order $T_{\mathrm{GG,z}} = 2\times10^{-3}$ Nm about the sail $\mathbf{z}$-axis.

A variable surface reflectivity distribution $0 \le \rho(s) \le 1$ will now be assumed to counteract this gravity gradient torque. The SRP force and torque about the sail's CoM are calculated using a simplified SRP model [1]. It assumes that the sail surface is a perfectly (specular) reflecting mirror, neglecting all other form of optical interactions between the solar photons and the sail surface such as diffuse reflection, absorption and thermal re-emission. It also does not account for wrinkles or sail billowing, and thus assumes a perfectly flat sail surface. Therefore, the SRP for reflectivity $\rho(s) = 1$ is

$$p_{\mathrm{SRP}} = 2p_0\left(\frac{R_{\mathrm{S,0}}}{R_{\mathrm{S}}}\right)^2\cos^2\alpha \tag{2}$$

at a radial distance R_{S} from the Sun, with the pitch angle α between the Sun-sail line and the sail plane normal and $p_0 = 4.563\times10^{-6}\ \mathrm{N/m^2}$ being the solar radiation pressure at $R_{\mathrm{S,0}} = 1$ AU.

When now assuming that the sail film reflectivity is no longer constant, but changes along the surface, the local SRP becomes a function of $\rho(s)$ as

$$p_{\mathrm{SRP}} = p_0 \left[1+\rho(s)\right] \left(\frac{R_{S,0}}{R_S} \right)^2 \cos^2 \alpha \tag{3}$$

where $\rho = 1$ represents the perfect mirror in Eq. (2) that experiences the maximum possible SRP load $p_{\max} = 2p_0$, while $\rho = 0$ reduces the effective SRP load to $p_{\max}/2 = p_0$, because only the momentum of the incoming photons is applying a force to the surface. As a consequence, the solar radiation pressure induced forces can be modified directly when changing the surface reflectivity.

According to Fig. 1, the incremental SRP force and torque acting about the CoM on a rectangular sail surface element can now be written as

$$dF_{\mathrm{SRP}} = p_0 L \left[1+\rho(s)\right] \left(\frac{R_0}{R_{\mathrm{S}}} \right)^2 \cos^2\alpha \; ds \tag{4}$$

$$dT_{\mathrm{SRP,z}} = p_0 L \left[1+\rho(s)\right] \left(\frac{R_0}{R_{\mathrm{S}}} \right)^2 \cos^2\alpha \; s\, ds \tag{5}$$

Assuming a linear reflectivity function

$$\rho(s) = a_0 + a_1 \cdot s \tag{6}$$

the above equations can be integrated over the interval $\left[-L/2, L/2\right]$, while constraining the sail surface to be always perpendicular to the Sun-sail line, thus $\alpha = 0$, and assuming that the solar distance $R_{\mathrm{S}} = 1\ \mathrm{AU}$ is constant on the Earth-centered orbit. The resulting SRP force and torque are found to be

$$F_{\mathrm{SRP}} = p_0 L \int_{-L/2}^{L/2} \left[1+a_0+a_1 \cdot s\right] ds \; = p_0 L^2 \left[1+a_0\right] \tag{7}$$

$$T_{\mathrm{SRP,z}} = p_0 L \int_{-L/2}^{L/2} \left[1+a_0+a_1 \cdot s\right] s \; ds = \frac{1}{12} p_0 L^4 a_1 \tag{8}$$

It can be seen that the magnitude of the resulting SRP force is only a function of the absolute coefficient a_0 . Furthermore, the SRP torque only depends on the gradient of the linear reflectivity function across the film, thus the difference of SRP force on the left and right hand side of the sail. If the forces are equal on both sides $(\mathrm{a}_1 = 0)$, the torque on the sail is clearly zero, regardless of the absolute value of the SRP force, as determined by a_0 .

Equation (8) represents the SRP torque that must be generated in order to counteract the gravity-gradient torque $T_{\mathrm{GG,z}}$ along the orbit, thus $T_{\mathrm{SRP,z}}$ must always be equal $T_{\mathrm{GG,z}}$. Thus, the coefficients a_i of the linear reflectivity function $\rho(s)$ can in general be calculated using the following equations

$$a_1 = \frac{12 T_{\mathrm{GG,z}}}{p_0 L^4}, \qquad a_0 = \frac{F_{\mathrm{SRP}}}{p_0 L^2} - 1 \tag{9}$$

Although a_1 is always determined through the current $T_{\mathrm{GG,z}}$ that needs to be compensated, a_0 is in principle only constrained by the maximum possible $F_{\mathrm{SRP,\,max}} = 2 p_0 L^2$, for which $a_0 = 1$ and also $\rho(s) = 1 = \text{const.}$ across the surface. However, a reflectivity gradient $a_1 \neq 0$ is necessary to create a torque, while at the same time $\rho(s) \leq 1$ across the entire sail. Thus, the upper constraint is $a_{0,\max} < 1$. The lower constraint is determined through the additional condition $\rho(L/2) = 0$ or $\rho(-L/2) = 0$ at the edge of the sail, in order to fix the linear reflectivity curve across the film. Inserting this into the linear reflectivity function (Eq. (6)), while keeping a_1 fixed, results in $a_{0,\min} = \pm a_1 (L/2)$ as the lower limit, depending on the sign of the torque that needs to be created. Since always $\rho(s) > 0$, this second condition also defines the minimum reflectivity distribution that likewise matches the torque requirement. Fig. 3 shows the resulting minimum reflectivity distribution $\rho(s)$ along the film as a function of the sail attitude angle γ during one revolution along the orbit for the chosen sail configuration.

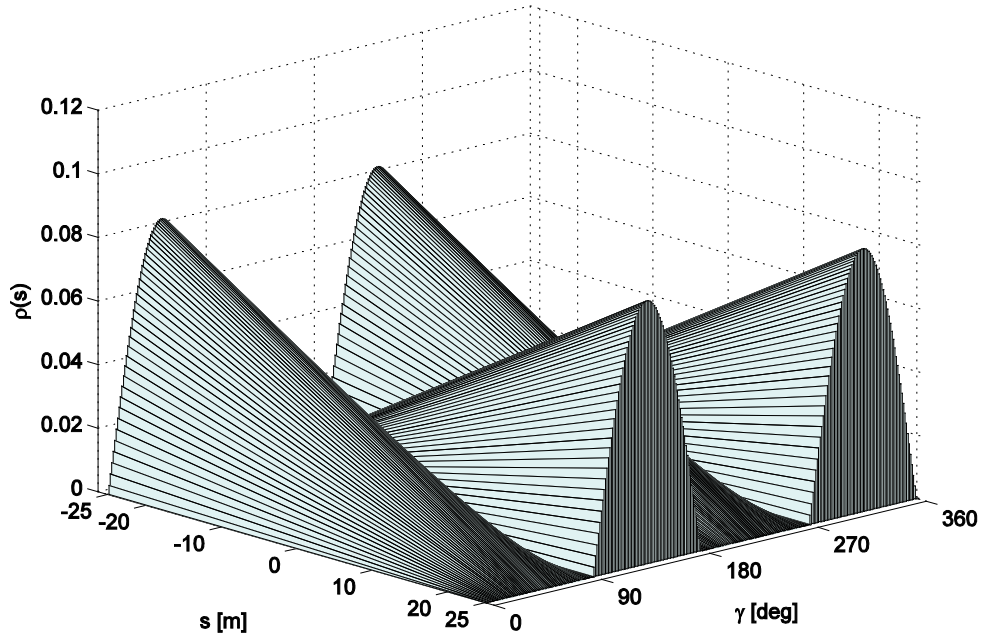

Fig. 3 Reflectivity distribution along a square rigid sail (*L* = 50 m) as function of sail attitude angle γ during one revolution along a 400-km LEO

III. Sail Shape Control using Variable Reflectivity Distribution

As mentioned in the introduction, a variable SRP reflectivity distribution can also be used to create desirable film deflections of a flexible circular disk sail. For that investigation, the sail is modeled with the same Kapton film used in section II, supported by a circumferential hoop structure, forming hinged-support type boundary conditions at the edges. Electro-chromic elements are again assumed to be distributed across the surface, as shown schematically in Fig. 4. For now, only the structural bending of the sail film is accounted for, ignoring time-dependent orbital and attitude dynamics of the structure due to distributed SRP forces and torques.

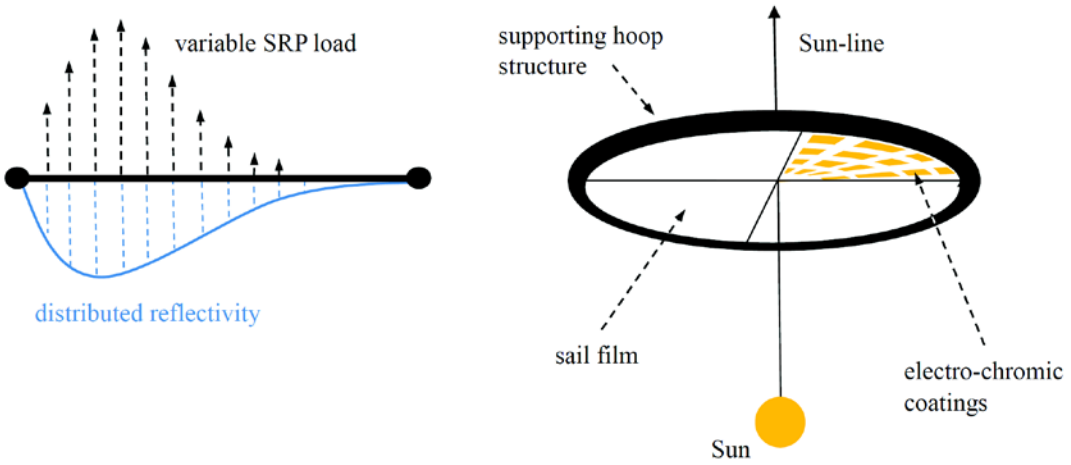

Fig. 4 Schematic of circular disk sail with electro-chromic coatings distributed across the surface (left) and supporting hoop structure (right)

In general, the SRP load distribution across the sail surface of diameter D causes an out-of-plane deflection w of the sail film from its initial flat shape. Due to the very small thickness, d, of the film material and relatively large deflections, w, (i.e. a high $W = w/d$ ratio), the non-linear theory of circular membranes needs to be used: in general, thin membrane-like structures offer a very small flexural rigidity and therefore cannot resist bending loads [7]. Furthermore, in-plane radial and transversal tension stresses are non-negligible, while for low W ratios these can be assumed negligible within the well-known linear beam theory [8]. Figure 5 shows a circular sail film of radius R and thickness d, under a uniform transverse SRP load $p_w = p_{SRP}$ perpendicular to the surface, initial radial in-plane tension $N_{r,0}$ at the edges and central deflection w_0.

The symmetrical out-of-plane deflection w can be described as a system of non-linear coupled ODEs of 2nd order. According to [9] these can be written in non-dimensional form as

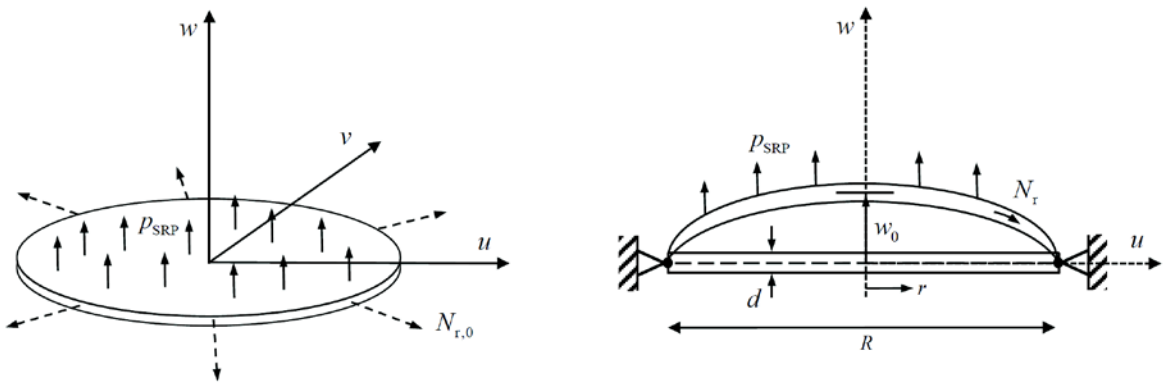

Fig. 5 Circular disk sail with transverse SRP load and initial in-plane tension (left) and sail film cross-section with hinged-edge support and deflected shape (right)

$$\xi^2\ddot{\theta}+\xi\dot{\theta}-[1+\xi^2(k^2+12(1-\upsilon^2)S_r)]\theta=6(1-\upsilon^2)P_{\mathrm{SRP}}\xi^3 \tag{10}$$

$$\xi^2\ddot{S}_r+3\xi\dot{S}_r=-\frac{1}{2}\theta^2 \tag{11}$$

where the following non-dimensional variables are used

$$\xi=\frac{r}{R},\ (\dot{})=\frac{d}{d\xi},\ W=\frac{w}{d},\ \mathrm{U}=\frac{u}{d} \tag{12}$$

$$\theta=\frac{dW}{d\xi}=\frac{R}{d}\frac{dw}{dr},\ \mathrm{S}_r=\frac{N_rR^2}{Ed^3} \tag{13}$$

with r the radial distance from the center of the sail disk, the dimensional radial in-plane tension N_r and in-plane deflection u. Furthermore, the non-dimensional parameters

$$k=\sqrt{\frac{N_{\mathrm{r},0}R^2}{D}}\ \text{ and }\ P_{\mathrm{SRP}}=\frac{p_{\mathrm{SRP}}R^4}{Ed^4} \tag{14}$$

denote the tension parameter k and the loading parameter P_{SRP} , using the Young's modulus E , Poisson ratio υ and the flexural rigidity

$$D=\frac{Ed^3}{12(1-\upsilon^2)} \tag{15}$$

of the sail film material. Within the scope of this paper, no initial in-plane tension $N_{\mathrm{r},0}$ has been accounted for to maximize the deflection, so the parameter k is zero. The corresponding boundary conditions (BC) to solve the boundary value problem (BVP) for a hinged edge support are then

$$\left.\begin{aligned}\theta&=0\\ S_r&=0\end{aligned}\right\}\ \text{for}\ \xi=0\quad\text{and}\quad\left.\begin{aligned}\dot{\theta}&=0\\ \dot{S}_r+(1-\upsilon)S_r&=0\end{aligned}\right\}\ \text{for}\ \xi=1 \tag{16}$$

This type of support was chosen to represent the real conditions in the best way, since the (almost rigid) hoop structure inhibits sail film deflections in the u direction, but allows for a non-zero slope $dW/d\xi$ at the edges.

In principle, the above BVP can be solved for any radially-symmetric load distribution $P_{\mathrm{SRP}}(\xi)$, whereas in the literature P is widely assumed to be constant across the film surface. Later in this section, variable load distributions $P(\xi)$ will be used to change the nominal deflection curves of sail films subjected to constant pressure loads P, as used, for example, in microelectronics and microfluidics [10]. After the BVP has been solved for $\theta(\xi)$, the vertical sail film deflection is obtained by integration from

$$W = \frac{w}{d} = \int \theta d\xi \tag{17}$$

The BVP is solved with the MATLAB™ bvp4c routine, using the three-stage Lobatto IIIa collocation method [11]. It is validated using the results observed in [10] for Silicon Nitride membranes with a clamped-edge support under a constant vertical load $P(\xi)$, showing that the found deflections $w(\xi)$ and non-dimensional in-plane tensions $S_r(\xi)$ can be reproduced. Furthermore, the chosen analytical approach is validated with a numerical finite-element analysis (FEM) conducted in [12] using circular Mylar® films ($\rho = 1350\,kg/m^3$, $E = 3.5\times10^9\ N/m^2$, $\upsilon = 0.38$ and $d_{\mathrm{Mylar}} = 1.0\times10^{-6}$ m) of varying radius and thickness. Figure 6 shows the relative deflections w/R obtained when solving the coupled ODE system for a constant SRP load at 1 AU and using hinged edge support.

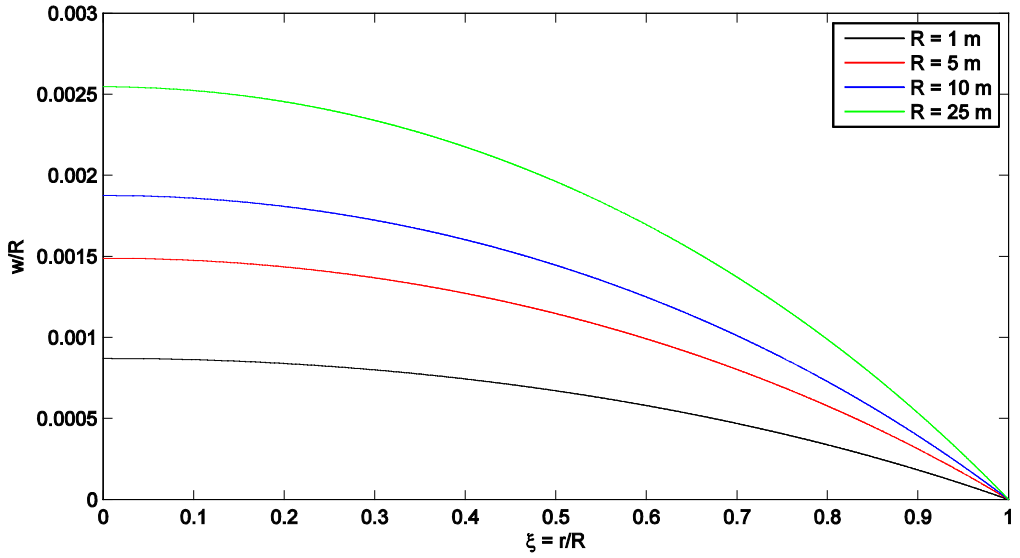

Fig. 6 Reproduction of relative out-of-plane deflections for Mylar sail films (thickness *d* = 1μm) at 1 AU for different sail disk radii found in [12]

The central sail film deflections are in the order of 0.2% of the sail disk radius and in good agreement with the results found in [12]. According to that analysis, the variation of load magnitude due the local deflection of the film was also taken into account. The film deflection changes the local light incidence angle, reducing the nominal SRP load. However, comparing results with [12] indicates that this effect is negligible, due to very small angular deflections of the surface.

A. Basic Sail Film Deflection for Constant Reflectivity

The material likely to be employed for future solar sails is Kapton®, due to its higher heat resistance and higher resistance to radiation compared to Mylar®. Accordingly, the deflection properties of a Kapton® film (thickness $d = 2.5\times10^{-6}\,\mathrm{m}$, density $\rho = 1572\,kg/m^3$, Young's Modulus $E = 2.48\times10^9\,N/m^2$ and Poisson ratio $\upsilon = 0.34$), according to [5], are investigated in the following. The sail surface is assumed to be always perpendicular to the Sun-sail line. Figures 7 and 8 show the relative sail film deflections w/R obtained for different sail disk sizes R = 1, 5, 10, 25, 50 and 100 m and for solar distances R_S = 0.5, 0.75, 1.0, 1.5, 2.5 and 3.0 AU, using a 100-m radius disk sail.

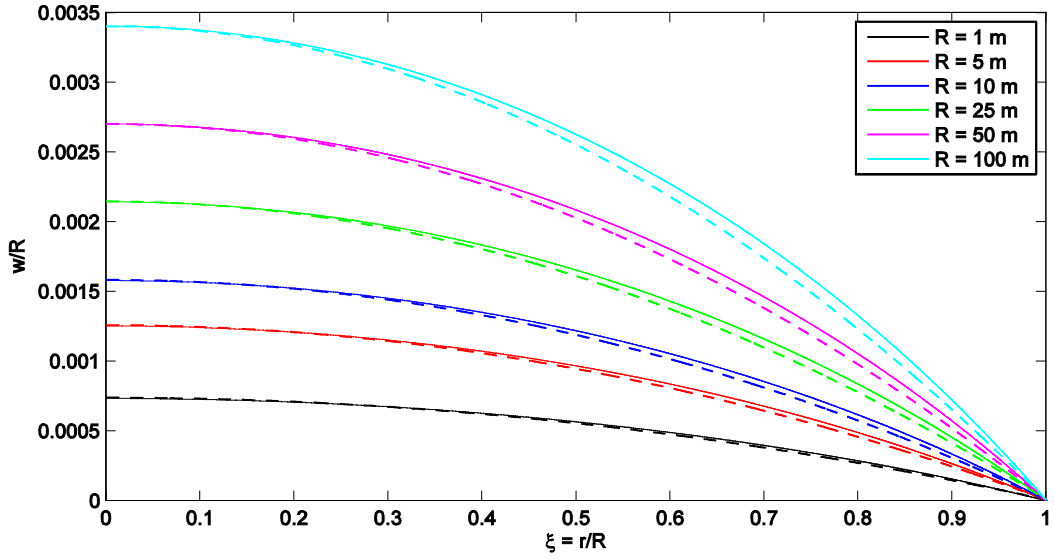

Fig. 7 Relative out-of-plane deflections for Kapton® sail film (thickness d = 2.5 µm) at 1 AU for different sail disk radii (solid lines) and hypothetic parabolic reference curves (dashed lines)

The dashed lines for each case indicate hypothetic parabolic reference curves that are satisfying the same boundary conditions and the same central deflections w_0/R. As can be seen, the deflection surfaces obtained are clearly not ideal paraboloids, as will be discussed below. The central deflections increase for larger sail disk sizes and smaller solar distances, as expected. In general, the absolute deflections stay below 0.5 m, even for

relatively large sail disks (100 m radius) and close to the Sun (0.5 AU), indicating large focal distances when using the sail film as a solar collector or antenna. The focal distances obtained will be discussed in section IV.

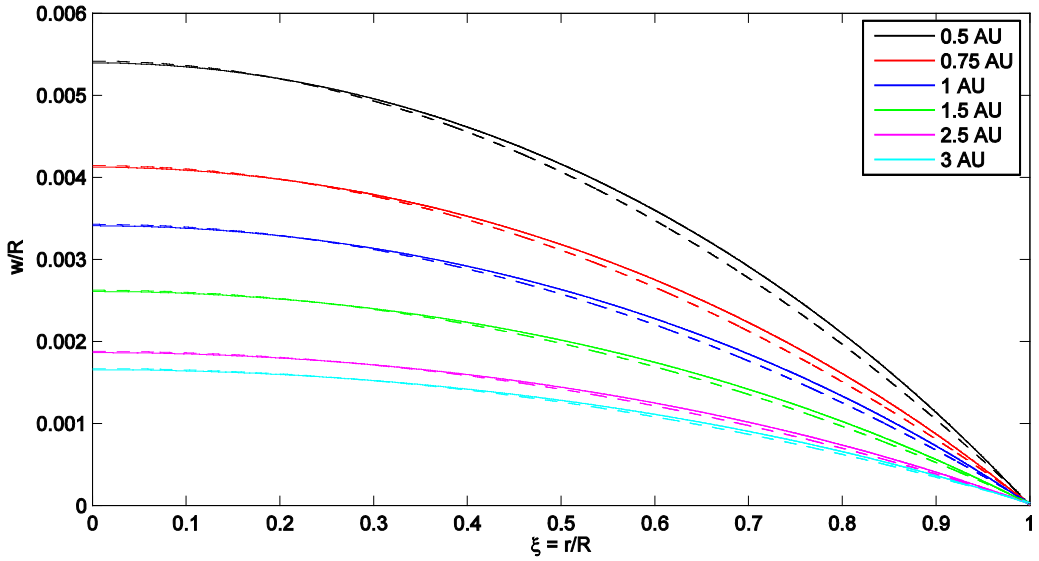

Fig. 8 Relative out-of-plane deflections for Kapton® sail film (radius R = 100 m, thickness d = 2.5 µm) at different Solar distances (solid lines) and hypothetic parabolic reference curves (dashed lines)

The trends of the relative central deflection w_0/R scale with $R^{1/3}$ for the sail disk radius and with $1/R_S^{2/3}$ for the solar distance, as can be seen in Fig. 9. The first result means that a larger disk radius is not necessarily beneficial, since the achievable sail deflections (and thus the focal length) are growing slower than the sail size. Furthermore, the deflection decreases slower than $1/R_S^2$ with solar distance, indicating moderate focal lengths are also available far from the Sun.

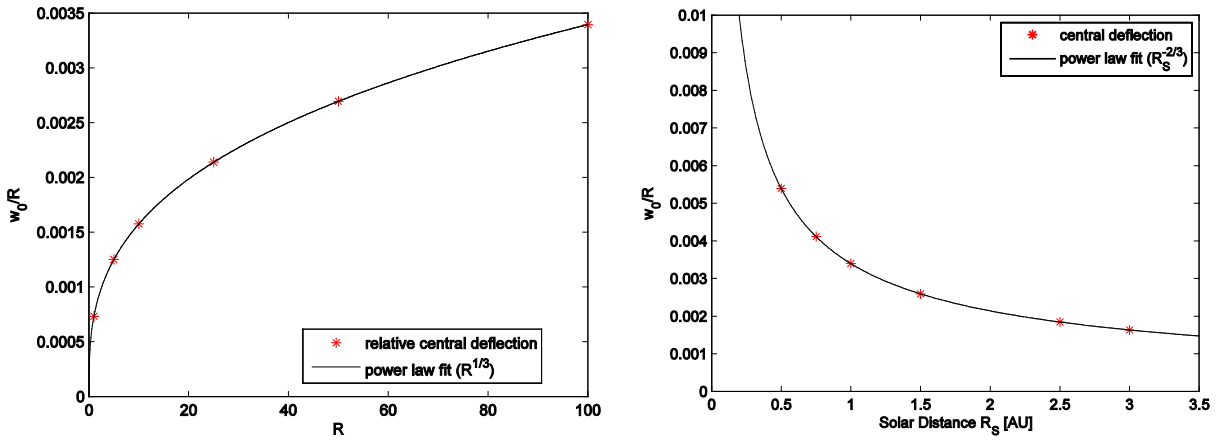

Fig. 9 Relative central sail deflections as function of sail disk radius R (left) and solar distance R_S (right), and power law fits to the data

When applying a polynomial fit to the sail deflection curves, a 3rd order (cubic) trend can be seen. This trend is shown in Fig. 10 for a 100-m radius sail disk at 1 AU, together with a parabolic fit using a 2nd order (parabolic) polynomial. Both polynomial fits are constrained to the central deflection value w_0/R.

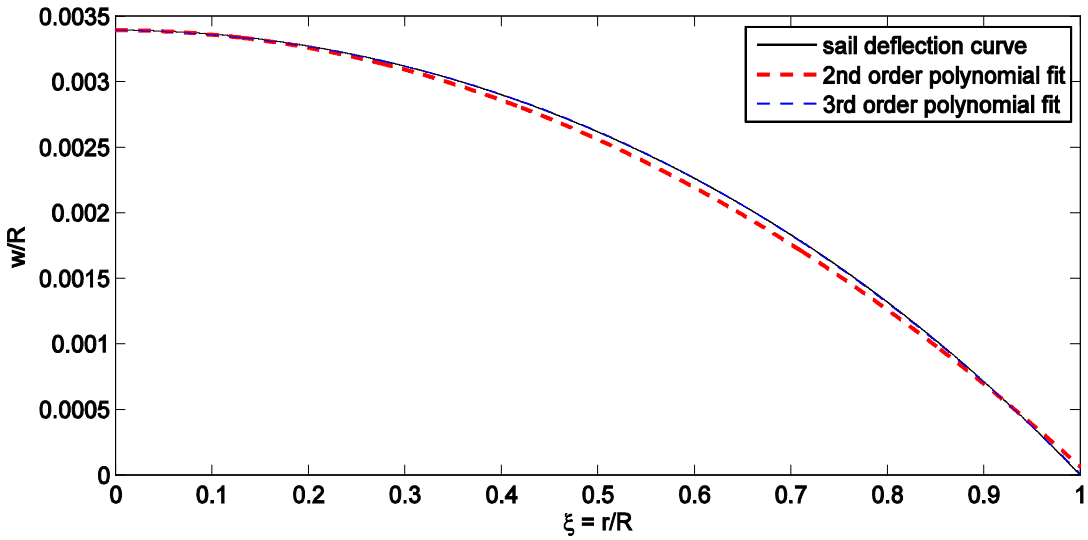

Fig. 10 Second and third order polynomial fits to sail film deflection curve, constrained to central deflection value

The cubic fit (solid blue line) is almost identical with the sail deflection curve (solid black line). Although the parabolic fit (dashed black line) does not match the BC at the edges exactly, the deviation of the sail deflection curve from the ideal parabolic shape is most visible in the mid-region of the sail disk. Here, the local gradient $dw/d\xi$ is smaller than the gradient of the parabola and vice-versa close to the edges. This indicates that the highly reflective Kapton® surface will not concentrate incoming light (or other forms of electro-magnetic radiation) into a single focal point due to aberration. In particular, the cubic surface reflects incoming light at the mid-part towards higher focal lengths and vice-versa for light impinging close to the edges. In the following, it will be shown that the cubic deflection can now be corrected to a parabolic one using a distributed reflectivity function across the sail surface.

B. Controlling Sail Film Deflection using Variable Reflectivity Distribution

In order to change the nominal (cubic) deflection shapes that are found for a constant SRP load distribution across the sail film, the surface reflectivity distribution needs to be controlled. As seen in Eq. (3), a modified SRP force model is employed throughout this study that incorporates the reflectivity $\rho(\xi)$ as a function of the position ξ along the sail surface

$$p_{\mathrm{SRP}}(\xi) = p_0\left[1+\rho(\xi)\right]\left(\frac{R_{S,0}}{R_S}\right)^2 \cos^2\alpha \tag{18}$$

When uniformly distributing electro-chromic elements across the sail disk, the reflectivity function $\rho(\xi)$ directly represents the SRP load distribution. Solving Eq. (19) for $\rho(\xi)$, while again assuming a constant pitch angle $\alpha = 0$, results as

$$\rho(\xi) = \frac{p_{\mathrm{SRP}}(\xi)}{p_0}\left(\frac{R_{S,0}}{R_S}\right)^{-2} - 1 \tag{19}$$

where an arbitrary load function $p_{\mathrm{SRP}}(\xi)$ can be used, as long as the physical constraint for $\rho(\xi) \in [0,1]$ is satisfied. We are now using this property to control the sail film shape, initially neglecting the additional mass and thickness that would be introduced to the sail film when distributing an electro-chromic coating layer on the surface.

Connecting $p_{\mathrm{SRP}}(\xi)$ with the non-dimensional load parameter P_{SRP} in Eq. (14) such that

$$P_{\mathrm{SRP}}(\xi) = \frac{p_{\mathrm{SRP}}(\xi)R^4}{Ed^4} \tag{20}$$

and substituting $P_{\mathrm{SRP}}(\xi)$ for the constant load distribution P_{SRP} within the coupled ODE system (Eq. (10)) introduces an arbitrary (radial symmetric) load function into the system that can be solved as a BVP, with corresponding boundary conditions at the center and at the edges.

Furthermore, an inverse problem can also be formulated, which is defined as calculating the necessary reflectivity function $\rho(\xi)$ to obtain a given sail deflection shape. This can, for example, be a parabolic shape in order to use the sail film as a large antenna. A parabolic deflection curve, as used already in Figs. Fig. 7 and Fig. 8, is of the general form

$$W_{\mathrm{parab}}(\xi) = -A\xi^2 + B\xi + C \tag{21}$$

where again $W = w/d$. When inserting the ideal parabolic curve into the coupled ODE system, it can be solved for $P_{\mathrm{SRP}}(\xi)$ in order to obtain the load distribution necessary to create this curve. Rearranging Eq. (10) for $P_{\mathrm{SRP}}(\xi)$ and Eq. (11) for the non-dimensional in-plane tension $S_{\mathrm{r}}(\xi)$ gives

$$P_{\mathrm{SRP}}(\xi) = \frac{1}{\upsilon^*}\left[\frac{\dddot{W}}{\xi} + \frac{\ddot{W}}{\xi^2} - [1+\xi^2(k^2+2\upsilon^* S_r)]\frac{\dot{W}}{\xi^3}\right] \tag{22}$$

$$\ddot{S}_r = -\frac{3}{\xi}\dot{S}_r - \frac{1}{2\xi^2}(\dot{W})^2 \tag{23}$$

using the Poisson parameter $\upsilon^* = 1-\upsilon^2$. Inserting the parabolic curve $W_{\text{parab}}(\xi)$ for *W*, the above equations now become

$$P_{\text{SRP}}(\xi) = -\frac{B}{\upsilon^*}\frac{1}{\xi^3} + 4AS_r - 2BS_r\frac{1}{\xi} \tag{24}$$

$$\ddot{S}_r = -\frac{3}{\xi}\dot{S}_r - \frac{B^2}{2\xi^2} - 2A^2 + 2AB \tag{25}$$

Now, Eq. (26) can be generally solved for S_r, without specifying boundary conditions

$$S_r = -\frac{1}{4}A^2\xi^2 + \frac{2}{3}AB\xi - \frac{C_1}{2\xi^2} - \frac{B^2}{4}\ln\xi + \frac{B^2}{8} + C_2 \tag{26}$$

When using again boundary conditions for hinged edge support, the above equation results in

$$S_r = -\frac{1}{4}A^2\xi^2 + \frac{2}{3}AB\xi - \frac{B^2}{4}\ln\xi + 1.0076A^2 - 1.6768AB + 0.3788B^2 \tag{27}$$

Inserting Eq. (28) into Eq. (25), the load distribution associated to a general parabolic deflection curve can now be written as

$$P_{\text{SRP}}(\xi) = -\frac{B}{\upsilon^*}\frac{1}{\xi^3} + \left(4A - \frac{2B}{\xi}\right)\left(-\frac{1}{4}A^2\xi^2 + \frac{2}{3}AB\xi - \frac{B^2}{4}\ln\xi + 1.0076A^2 - 1.6768AB + 0.3788B^2\right) \tag{28}$$

It can be seen that $P_{\text{SRP}}(\xi)$ is fully determined by the polynomial coefficients A and B.

The inverse problem is now applied to create a parabolic deflection shape for a 100-m disk sail of thickness $d = 2.5\times10^{-6}$ m at 1 AU. Fig. 11a) shows the nominal cubic deflection for constant reflectivity, thus a uniform load distribution. Furthermore, a parabolic reference deflection curve (dashed black line) of the simplified form

$$W_P(\xi) = -A\xi^2 + C \tag{29}$$

is taken as input for the inverse problem. The coefficient A is the slope and C is the vertex of the parabola. The parameter B is zero, thus $W_P(\xi)$ has no horizontal offset from the symmetry axis. In order to match the central deflection of the nominal cubic deflection curve and the zero-deflection condition at the edges, the coefficients are chosen to be $A = C = W_{0,\text{nom}}$, where $W_{0,\text{nom}}$ represents the central deflection obtained for constant reflectivity.

Accordingly, the parabolic reference curve is now

$$W_P(\xi) = -W_{0,\text{nom}}\xi^2 + W_{0,\text{nom}} \tag{30}$$

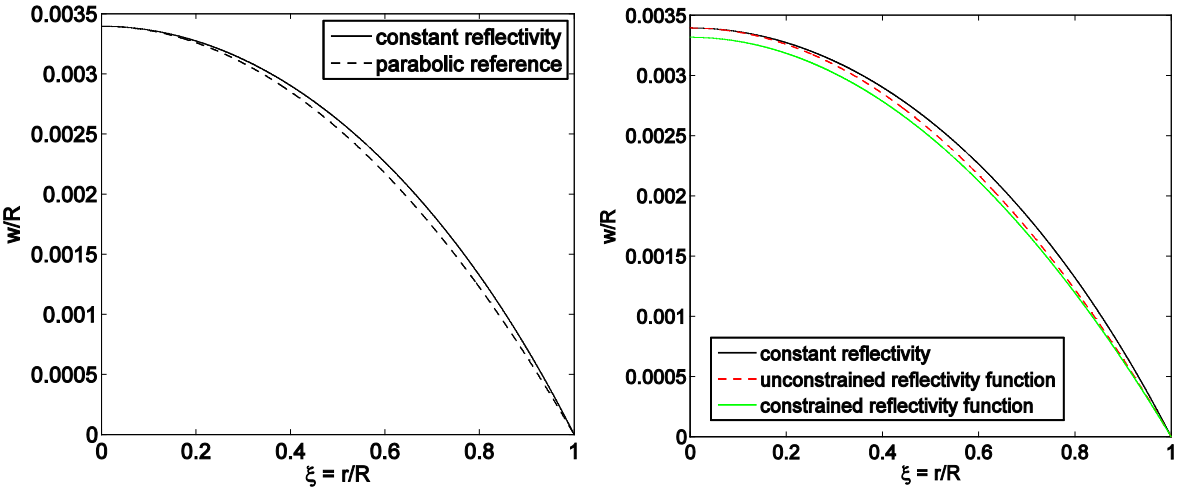

a) **b)**

Fig. 11 a) Nominal deflection curve for constant surface reflectivity using 100-m disk sail (thickness $d = 2.5$ µm) at 1 AU (solid line) and parabolic reference curve (dashed line). b) Unconstrained parabolic deflection curve (dashed red line) and constrained parabolic curve (dashed green line)

After inserting the reference parabola $W_P(\xi)$ into Eq. (29), the $P_{\mathrm{SRP}}(\xi)$ function becomes

$$P_{\mathrm{SRP}}(\xi) = 4W_{0,\mathrm{nom}}\left(-\frac{1}{4}W_{0,\mathrm{nom}}^2\xi^2 + 1.0076\ W_{0,\mathrm{nom}}^2\right) \tag{31}$$

and simplifies to

$$P_{\mathrm{SRP}}(\xi) = W_{0,\mathrm{nom}}^3\left(4.0304 - \xi^2\right) \tag{32}$$

When introducing this $P_{\mathrm{SRP}}(\xi)$ function into the coupled ODE system, it can be solved as a regular BVP. As can be seen in Fig. 11b), the resulting deflection curve (dashed red line) exactly matches the input curve in Fig. 11a). When reformulating Eq. (33) , the absolute SRP load distribution can be written as

$$p_{\mathrm{SRP}}(\xi) = \frac{Ed^4}{R^4}W_{0,\mathrm{nom}}^3\left(4.0304 - \xi^2\right) \tag{33}$$

However, the $p_{\mathrm{SRP}}(\xi)$ distribution does not necessarily match the condition not to exceed the maximum possible $p_{\max} = 2p_0\left(R_{S,0}/R_S\right)^2$ at a certain solar distance or, equivalently, not to exceed the maximum reflectivity $\rho_{\max}(\xi) = 1$. As can be seen in Fig. 12, the normalized load distribution $p_{\mathrm{SRP}}(\xi)/p_0$ for the chosen case exceeds $p_{\max}/p_0 = 2\left(R_{S,0}/R_S\right)^2$, showing that it is not possible to achieve the same nominal central deflection when simply constraining the sail film to a parabolic deflection. After introducing the additional

constraint $p_{\mathrm{SRP}}(\xi) \le p_{\max}$ into the SRP load function, the coefficients $A_C = C_C = W_{0,C}$ for the constrained parabola can be calculated from Eq. (34) as

$$W_{0,C} = \left(\frac{2 p_0 R^4}{4.0304 E d^4} \left(\frac{R_{S,0}}{R_S} \right)^2 \right)^{\frac{1}{3}} \tag{34}$$

In here, the constrained central deflection $W_{0,C}$ is now fully determined by the sail film parameters, the sail disk size and the solar distance. The constrained load distribution is also shown in Fig. 12 (green solid curve).

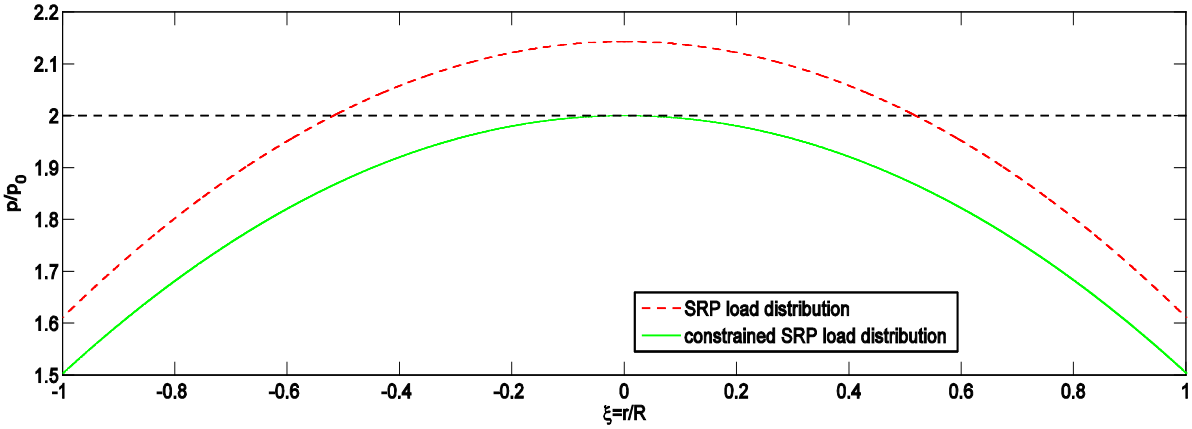

Fig. 12 Non-dimensional load distribution for unconstrained parabolic deflection curve (dashed red line) and for constrained parabolic deflection (solid green line)

The constrained parabolic deflection curve is also shown in Fig. 11b) (dashed green line); its central deflection is about 3% smaller compared to the unconstrained parabolic deflection curve (dashed red line).

The corresponding reflectivity distribution $\rho(\xi)$, according to Eq. (20), is finally found after inserting the SRP load distribution of Eq. (34)

$$\rho(\xi) = \frac{E d^4}{p_0 R^4} \left(\frac{R_S}{R_{S,0}} \right)^2 W_{0,\mathrm{C}}^3 \left(4.0304 - \xi^2 \right) - 1 \tag{35}$$

Inserting the constraint for the central deflection $W_{0,\mathrm{C}}$ into Eq. (36) results in

$$\rho(\xi) = 1 - \frac{2}{4.0304} \xi^2 \tag{36}$$

It can be seen that the reflectivity distribution in order to create a parabolic deflection shape is independent of the sail film parameters and solar distance. The reflectivity distribution is visible in Fig. 13, along with the constrained distribution that abides by $\rho \le 1$.

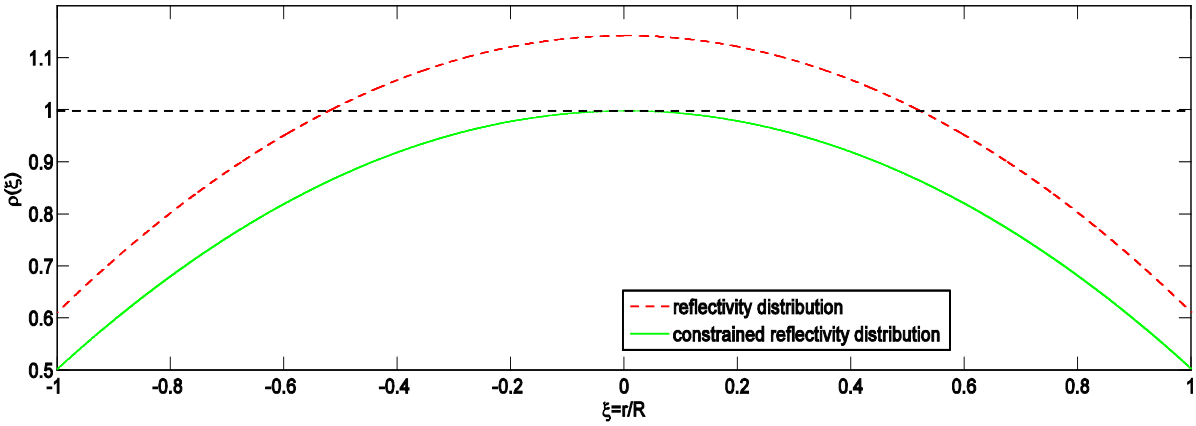

Fig. 13 Reflectivity distribution for unconstrained parabolic deflection curve (dashed red line) and distribution for constrained parabolic deflection (solid green line)

In summary, the necessary reflectivity distribution in order to create a parabolic sail film deflection is independent of the disk radius, film thickness and solar distance. The magnitude of central sail film deflection can be calculated analytically for a circular sail of radius R and film thickness d, perpendicular to the Sun at a solar distance R_S.

IV. Computation of Focal Length of Parabolic Sail Reflector

It was shown in the preceding section that the deflection curve of a sail film exposed to SRP can be controlled by changing the reflectivity distribution across the surface. Accordingly, the nominal deflection shape due to a constant reflectivity distribution, which is normally a cubic polynomial function, can be transformed into a true parabolic shape. A large, highly reflective parabolic surface has many potential applications, such as communication, sensing and power collection. In order to evaluate the usefulness of the shapes that can be generated, some properties of parabolic reflectors have to be identified.

A paraboloid concentrates the incoming electro-magnetic radiation into a single focal point, depending on the geometrical precision of the surface generated. When approximating the nominal cubic deflection shapes calculated in Section III by a parabolic curve $W_P = A\xi^2 + C = W_{0,C}\xi^2 + W_{0,C}$, the corresponding focal lengths, thus the focal distance from the vertex of the parabola, can be calculated as

$$f = \frac{1}{4A} = \frac{1}{4W_{0,C}} \tag{37}$$

using the central deflection $W_{0,C}$ of the constrained parabola, as it was shown in Eq. (35). When transforming the parabolic function W_P into dimensional form

$$w_P = W_{0,\mathrm{C}} d \left(\frac{r}{R} \right)^2 + W_{0,\mathrm{C}} d = \frac{W_{0,\mathrm{C}} d}{R^2} r^2 + W_{0,\mathrm{C}} d = a r^2 + c \tag{38}$$

where $a = W_{0,\mathrm{C}} d / R^2 = w_{0,\mathrm{C}} / R^2$ and $c = W_{0,\mathrm{C}} d = w_{0,\mathrm{C}}$, thus the focal length is now

$$f = \frac{1}{4a} = \frac{R^2}{4 w_{0,\mathrm{C}}} \tag{39}$$

The resulting focal lengths for the deflected circular disk sails calculated in Section III are shown in Fig. 14 as a function of disk radius and solar distance. The results are in good agreement with [12].

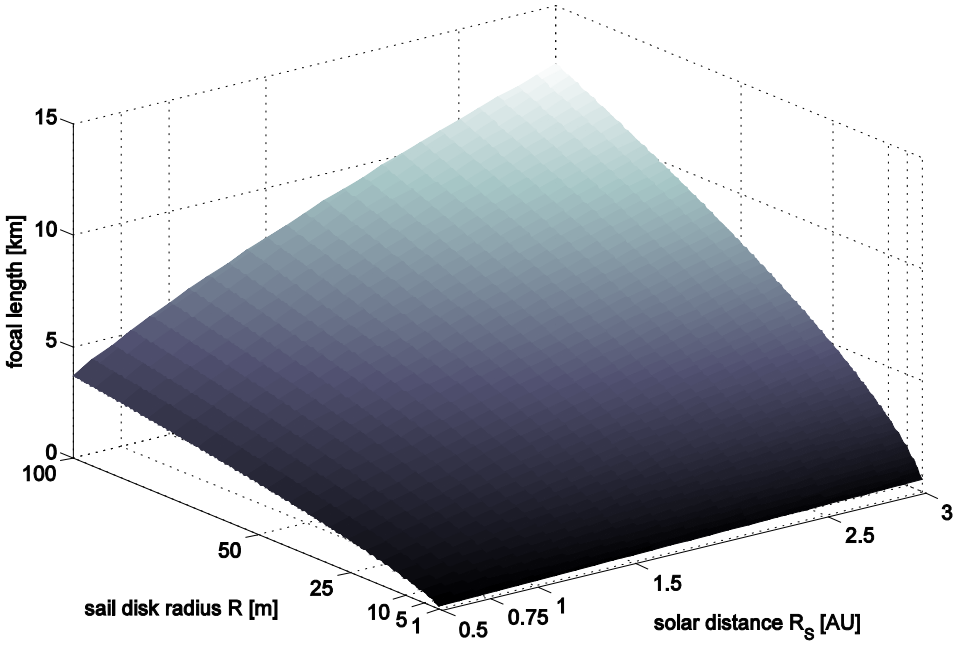

Fig. 14 Focal length of parabolic reference deflection curve of a circular solar sail disk as a function of disk radius and solar distance

For example, a circular disk sail of 100 m radius at 1 AU has a focal length $f_{100} = 5.98$ km. When positioning a detached platform at the focus, and so formation-flying with the solar sail, the platform will be at the focus of a large true antenna, or will be at the focus of a power collector.

V. Conclusion

A variable reflectivity distribution across the surface of a thin Kapton® sail film has been used to investigate potentially novel mission applications for solar sails. The surface reflectivity can be manipulated when distributing electro-chromic elements across the sail film that change their reflectivity according to an applied electric potential. First, a linear reflectivity function was employed to control the attitude of a solar sail in low

Earth orbit. In particular, the steering method has been applied to counteract the gravity-gradient torques acting on a large rigid sail film. It was shown that a constant Sun-pointing attitude can be maintained along the orbit, while simultaneously minimizing the necessary surface reflectivity variation.

Furthermore, a variable reflectivity distribution has been used to change the deflection shape of a flexible circular sail film, supported by a rigid hoop structure around the edge. The nominal sail film deflection due to a constant solar radiation pressure load distribution perpendicular to the surface has been calculated for various sail disk radii and solar distances, using non-linear theory of thin circular membranes. The results indicate that the deflected sail film surface does not concentrate incoming light (or other forms of electro-magnetic radiation) into a single focal point due to non-parabolic aberration. However, an analytical expression for the reflectivity function across the surface necessary to create a true parabolic deflection shape has been derived. This radially symmetric reflectivity function does not depend on sail size, film material or solar distance. Although limited to sail films perpendicular to the Sun-sail line, this can be used for prefabricating a fixed reflectivity distribution on the film surface. In space, this allows the solar sail to obtain a parabolic film deflection at any solar distance. Although the focal length will be changing, this can be compensated by a detached platform formation-flying in the current focus.

The focal length of the resulting parabolic reflector can be calculated using the derived analytical function. It was shown that the focal length increases with sail radius and solar distance.

Throughout this preliminary analysis, simplifying assumptions have been made such as neglecting the additional mass and thickness that would be introduced to the sail film when distributing an electro-chromic coating layer on the surface. Accordingly, extending the non-linear approach to incorporate multi-layer composite membranes will result in better estimates of the actual deflection shapes. Furthermore, no initial billowing of the sail film has been accounted for, as it is assumed to be kept flat by the hoop structure. Thus, only the flexible structural bending has been accounted for so far, which has shown to lead towards relatively small film deflections and thus long focal lengths. Incorporating an initial ‘floppiness’ of the sail film, the dynamical inflation of the film prior to flexible bending can be used to increase the overall deflection and to create shorter focal lengths and thus a higher performance of an optical sail reflector.

Acknowledgments

This work was funded by the European Research Council Advanced Investigator Grant VISIONSPACE: Orbital Dynamics at Extremes of Spacecraft Length-Scale (227571).

References

1. C. R. McInnes, “Solar sailing: technology, dynamics and mission applications”, *Springer-Praxis books in astronautical engineering*, ed. J. Mason, Springer-Verlag, Berlin, 1999. ISBN: 3-540-21062-8
2. C. R. McInnes, “Delivering fast and capable missions to the outer solar system”, *Advances in Space Research*, vol. 34, n. 1, p. 184-191, 2004. DOI: 10.1016/j.asr.2003.02.063
3. H. Demiryont, D. Moorehead, “Electrochromic emissivity modulator for spacecraft thermal management”, *Solar Energy Materials and Solar Cells*, vol. 93, n. 12, p. 2075-2078, 2009. DOI: 10.1016/j.solmat.2009.02.025
4. S. Timoshenko, S. Woinowsky-Krieger, “Theory of plates and shells”, McGraw-Hill, 1959.
5. D. W. Sleight, D. M. Muheim, “Parametric studies of square solar sails using finite element analysis”, in *Proceedings of Collect. of Pap. - 45th AIAA/ASME/ASCE/AHS/ASC Struct., Struct. Dyn. and Mater. Conf.; 12th AIAA/ASME/AHS Adapt. Struct. Conf.; 6th AIAA Non-Deterministic Approaches Forum; 5th AIAA Gossamer Spacecraft Forum, April 19, 2004 - April 22, 2004*, Palm Springs, CA, United states, 2004.
6. H. Schaub, J. L. Junkins, “Anayltical Mechanics of Space Systems”, American Institute of Aeronautics and Astronautics, 2009. ISBN: 9781600867217
7. E. Ventsel, T. Krauthammer, “Thin Plates and Shells: Theory: Analysis, and Applications”, Taylor & Francis, 2001. ISBN: 9780824705756
8. R. R. Craig, “Mechanics of Materials”, John Wiley & Sons, 2011. ISBN: 9780470481813
9. J. A. Voorthuyzen, P. Bergveld, “The influence of tensile forces on the deflection of circular diaphragms in pressure sensors”, *Sensors and Actuators*, vol. 6, n. 3, p. 201-213, 1984. DOI: http://dx.doi.org/10.1016/0250-6874(84)80021-9
10. M. J. D. Sheplak, “Large Deflections of Clamped Circular Plates Under Initial Tension and Transitions to Membrane Behavior”, *Journal of Applied Mechanics, Transactions ASME*, vol. 65, n. 1, p. 107-115, 1998. DOI: 10.1115/1.2789012
11. L. F. Shampine, I. Gladwell, S. Thompson, “Solving ODEs with MATLAB”, Cambridge University Press, 2003. ISBN: 9780521530941
12. F. Couceiro, P. V. Gamboa, J. M. Silva, A. D. Guerman, “Configuration of a thin circular membrane subject to solar pressure”, in *Proceedings of 2012 International Conference on Spacecraft Structures, Materials and Mechanical Testing, ICSSMMT 2012, December 27, 2012 - December 28, 2012*, Xiamen, China, 2013. DOI: 10.4028/www.scientific.net/AMM.290.47